Dynamic Stability of a Rectangular Plate with Four Free Edges Subjected to a Follower Force

Ken Higuchi* and Earl H. Dowell†
Duke University, Durham, North Carolina 27706

The dynamic stability of a flexible rectangular plate, such as a plate-like large space structure, is analyzed. One of the four free edges of the plate is subjected to a tangential follower force. The plate shows both flutter and divergence instabilities. The flutter load and divergence load are obtained for various slenderness ratios of the rectangular plate by means of modal analysis. In the calculation, many weak instabilities were found; a weak instability sometimes corresponds to a critical load which is significantly smaller than the strong flutter load. The flutter mechanism was studied in depth because the behavior of flutter is fairly complicated with respect to variations in slenderness ratio. Moreover, it was determined that a smaller slenderness ratio is generally desirable to realize a high acceleration of the plate.

Nomenclature

a	= length of the plate, (see Fig. 1)
b	= width of the plate, (see Fig. 1)
D	= bending rigidity of the plate
$\overline{G_{mnij}}$	= element of nondimensional load matrix
K_{mnij}	= element of stiffness matrix
$\overline{K_{mnij}}$	= element of nondimensional stiffness matrix
M_{mnij}	= element of mass matrix
$\overline{M_{mnij}}$	= element of nondimensional mass matrix
$\bar{m}$	= surface density
Q	= nondimensional follower force, [see Eq. (37)]
Q_D	= nondimensional divergence load
Q_F	= nondimensional flutter load
Q_{ij}	= generalized force, [see Eq. (12)]
Q_{mnij}	= element of generalized force, [see Eq. (11)]
q	= follower force per unit width
T	= kinetic energy
t	= time
U	= strain energy
$W_{mn}(t)$	= generalized coordinate, [see Eq. (5)]
$\overline{W_{mn}}$	= see Eq. (15)
$w(x,y,t)$	= deflection
$X_m(x)$	= coordinate function in the direction of x
$\overline{X_m(\xi)}$	= m-th free-free beam function in the direction of ξ
x,y	= coordinates, (see Fig. 1)
$Y_n(y)$	= coordinate function in the direction of y
$\overline{Y_n(\eta)}$	= n-th free-free beam function in the direction of η
α	= nondimensional acceleration, [see Eq. (39)]
β_m, β_n	= eigenvalues of a free-free beam, [see Eqs. (22) and (23), (26) and (27)]
$\nabla^2(\ )$	= $\partial^2(\ )/\partial x^2 + \partial^2(\ )/\partial y^2$
δ	= variation
$\bar{\delta}$	= Dirac's delta function
δ_{mi}, δ_{nj}	= Kronecker's deltas
δW_{NC}	= virtual work
$\lambda = a/b$	= slenderness ratio
ν	= Poisson's ratio
Θ	= direction parameter of the follower force, (see Fig. 1)
ω	= frequency, [see Eq. (15)]
$\Omega = \Omega_R \pm i\Omega_I$	= nondimensional frequency, [see Eq. (36)]
Ω_I	= imaginary part of Ω
Ω_R	= real part of Ω
ξ	= x/a
η	= y/b
$(\dot{\ })$	= $\partial(\ )/\partial t$
$(\ )'$	= derivative with respect to a spatial coordinate

Received March 7, 1988; presented as Paper 88-2412 at the AIAA/ASME/ASCE/AHS 29th Structure, Structural Dynamics and Materials Conference, Williamsburg, VA, April 18-20, 1988; revision received Nov. 28, 1988.

*Visiting Scholar at Duke University on leave from Tokyo Denki University, Japan. Member AIAA.

†Professor and Dean, Department of Mechanical Engineering and Materials Sciences. Fellow AIAA.

‡Note to the Reader: The terms "flutter" or "divergence" are used here to denote a dynamic instability or a static instability of a flexible structure under the action of a nonconservative force. In aerospace engineering literature, the source of the nonconservative force is often an aerodynamic flow. Here, the source is a follower force. For those readers familiar with the aerodynamic flutter and divergence literature but not the follower force literature, it may be noted that the basic dynamics and statics are similar. The flutter mechanism in follower force problems is almost invariably one of frequency coalescence, analogous to bending-torsion wing flutter in an aerodynamic flow. This is because the follower force itself is usually a static, rather than a time dependent, force. If the follower force was time dependent, other forms of flutter may also arise. The reader may wish to consult a standard reference for further details, for example, "A Modern Course in Aeroelasticity", edited by Sitjhoff and Noorhoff, 2nd Edition, by Dowell, Curtiss, Scanlan and Sisto, 1989.

I. Introduction

LARGE space structures will be constructed for low Earth orbit and then will be moved, for example, to a geostationary point. A plate-like large space structure, such as a solar power station, may undergo dynamic instabilities because of its low rigidity when it is thrusted by follower forces. Investigated here is the dynamic instability of a rectangular plate that has four free edges and is subjected to a follower force on one edge.

For a free-free beam (missile) subjected to an end thrust, the dynamic instability has been studied by several authors.[1-7] Beal,[1] using a Galerkin method, extensively investigated the problem including the effect of a control and a pulsating thrust. In later studies, Wu,[3] and Peters and Wu[4] stated that the second lowest branch of the eigenvalue curves determines the critical load. They demonstrated this numerically by using a finite-element method based upon an adjoint formulation. They further studied the mode shapes analytically by using

asymptotic expansions. Matsumoto and Mote,[5] Park and Mote,[6] and Park[7] considered a control system in order to increase the stability of the beam. The history of research on a free-free beam with distributed parameters subjected to an end thrust is discussed in Ref. 4. A free-free beam with nonconservative loading on both ends has also been studied.[8,9]

Celep[10,11] studied a circular plate with all free edges undergoing axisymmetric and asymmetric deformations and subjected to a nonconservative edge load. Of course, by definition, a circular plate is limited to a single slenderness ratio. For a rectangular plate, there are also some studies,[12-17] though none for all free edges. A cantilever plate[12] and a cantilever plate with simply supported two opposite sides[13,14] subjected to nonconservative edge loading on free edges were considered. Leipholz and Pfendt[17] investigated the stability formulation of a rectangular plate with various edge conditions subjected to follower forces uniformly distributed over the surface of the plate, by using an extended Galerkin equation. These studies are helpful in understanding the complicated characteristics of dynamic stability of plates under nonconservative forces. But none of their examples includes the case where all edges are free.

In this study, instability phenomena of the completely free edged plate thrusted by a compressive tangential force uniformly distributed on one edge are examined by means of modal analysis. Flutter load and divergence load are obtained for various slenderness ratios. And along with the change of the slenderness ratio, the mechanism of flutter is discussed. The effect of the true damping ratio on the flutter load is also investigated. Finally, the optimum slenderness ratio, where the largest acceleration can be realized without any instability, is determined.

II. Formulation

Hamilton's Principle

Hamilton's Principle can be written as

$$\int_{t_1}^{t_2}(\delta T - \delta U + \delta W_{NC})\mathrm{d}t = 0 \tag{1}$$

where kinetic energy T potential energy U and the virtual work done by nonconservative forces δW_{NC} are written as follows for a uniform, isotropic plate subjected to a follower force (Fig. 1).

$$U = \frac{1}{2}\int_0^b\int_0^a\left(D\left\{(\nabla^2 w)^2 + 2(1-\nu)\left[\left(\frac{\partial^2 w}{\partial x \partial y}\right)^2 - \frac{\partial^2 w}{\partial x^2}\frac{\partial^2 w}{\partial y^2}\right]\right\} - q\frac{x}{a}\left(\frac{\partial w}{\partial x}\right)^2\right)\mathrm{d}x\mathrm{d}y \tag{2}$$

$$T = \frac{1}{2}\int_0^b\int_0^a \bar{m}\left(\frac{\partial w}{\partial t}\right)^2 \mathrm{d}x\mathrm{d}y \tag{3}$$

$$\delta W_{NC} = -\int_0^b\int_0^a q(\Theta + 1)\frac{\partial w}{\partial x}\bar{\delta}(x-a)\delta w\,\mathrm{d}x\mathrm{d}y \tag{4}$$

where $w(x,y,t)$ is the plate deflection, and $\bar{\delta}(x-a)$ is Dirac's delta function. The magnitude of a compressive follower force per unit width uniformly distributed on the edge of $x = a$ is q; and the force direction of q varies, although the magnitude is invariant. The direction parameter based upon the angle between the force direction and a line tangential to the plate is represented by Θ (Fig. 1).

Rayleigh-Ritz Approach

A Rayleigh-Ritz approach is applied as follows.[18] By introducing the expansion of the plate deflection

$$w(x,y,t) = \sum_m\sum_n W_{mn}(t)X_m(x)Y_n(y) \qquad m,n = 1,2,3,\ldots \tag{5}$$

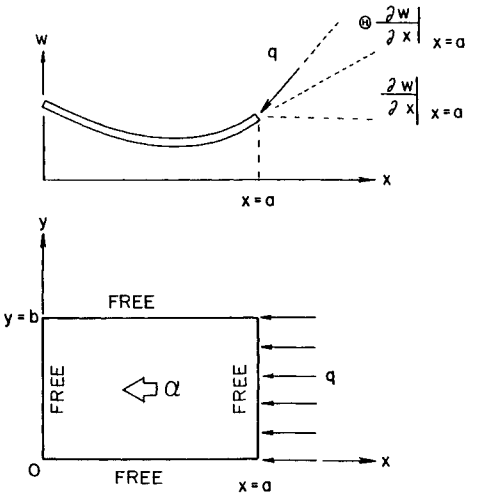

Fig. 1 Geometry.

we rewrite Eqs. (2-4) as follows:

$$T = \frac{1}{2}\sum_m\sum_n\sum_i\sum_j \dot{W}_{mn}\dot{W}_{ij}M_{mnij} \qquad m,n,i,j = 1,2,3,\ldots \tag{6}$$

$$U = \frac{1}{2}\sum_m\sum_n\sum_i\sum_j W_{mn}W_{ij}K_{mnij} \qquad m,n,i,j = 1,2,3,\ldots \tag{7}$$

$$\delta W_{NC} = -\sum_m\sum_n\sum_i\sum_j W_{mn}\delta W_{ij}Q_{mnij} \qquad m,n,i,j = 1,2,3,\ldots \tag{8}$$

where, M_{mnij}, K_{mnij}, and Q_{mnij} are the coefficients formed by integrating the coordinate functions in Eqs. (2-4), namely

$$M_{mnij} = \int_0^b\int_0^a \bar{m}X_mY_nX_iY_j\,\mathrm{d}x\mathrm{d}y \tag{9}$$

$$K_{mnij} = \int_0^b\int_0^a\Big(D\{(\nabla^2X_mY_n)(\nabla^2X_iY_j) + (1-\nu)[2X_m'Y_n'X_i'Y_j' - (X_m''Y_nX_iY_j'' + X_mY_n''X_i''Y_j)]\} - q(x/a)(X_m'Y_nX_i'Y_j)\Big)\,\mathrm{d}x\mathrm{d}y \tag{10}$$

$$Q_{mnij} = \int_0^b\int_0^a q(\Theta+1)X_m'Y_nX_iY_j\,\bar{\delta}(x-a)\,\mathrm{d}x\mathrm{d}y \tag{11}$$

The generalized force Q_{ij} for the ij-th generalized coordinate is

$$Q_{ij} = \sum_m\sum_n W_{mn}Q_{mnij} \tag{12}$$

Now we can obtain Lagrange's equation from Eqs. (1) and (6-12) as follows:

$$\frac{\mathrm{d}}{\mathrm{d}t}\left[\frac{\partial(T-U)}{\partial\dot{W}_{ij}}\right] - \frac{\partial(T-U)}{\partial W_{ij}} + Q_{ij} = 0 \quad i,j = 1,2,3,\ldots \tag{13}$$

or

$$\sum_m\sum_n(\ddot{W}_{mn}M_{mnij} + W_{mn}K_{mnij} + W_{mn}Q_{mnij}) = 0 \qquad m,n,i,j = 1,2,3,\ldots \tag{14}$$

Suppose that the vibration is stationary, i.e.,

$$W_{mn}(t) = \overline{W_{mn}}e^{i\omega t}, \qquad i^2 = -1 \tag{15}$$

then, we obtain the following eigenvalue problem:

$$\sum_m\sum_n \overline{W_{mn}}(-\omega^2M_{mnij} + K_{mnij} + Q_{mnij}) = 0 \qquad m,n,i,j = 1,2,3,\ldots \tag{16}$$

This eigenvalue problem involves the external force q implicitly in K_{mnij} and Q_{mnij} as shown in Eqs. (10) and (11).

Coordinate Functions

One may choose the mode functions of a free-free beam as the coordinate functions $X_m(x)$ and $Y_n(y)$.[19,20] Here, let us introduce the nondimensional coordinates as follows:

$$\xi = x/a \quad (0 \le \xi \le 1) \tag{17}$$

$$\eta = y/b \quad (0 \le \eta \le 1) \tag{18}$$

$$\lambda = a/b \tag{19}$$

$$\overline{X_1(\xi)} = 1 \tag{20}$$

$$\overline{X_2(\xi)} = \sqrt{3}(2\xi - 1) \tag{21}$$

$$\overline{X_m(\xi)} = (\mathrm{ch}\beta_m\xi + \cos\beta_m\xi) - \sigma_m(\mathrm{sh}\beta_m\xi + \sin\beta_m\xi) \tag{22}$$

where

$$\sigma_m = \frac{\mathrm{ch}\beta_m - \cos\beta_m}{\mathrm{sh}\beta_m - \sin\beta_m}, \qquad m = 3,4,5,\ldots \tag{23}$$

$$\overline{Y_1(\eta)} = 1 \tag{24}$$

$$\overline{Y_2(\eta)} = \sqrt{3}(2\eta - 1) \tag{25}$$

$$\overline{Y_n(\eta)} = (\mathrm{ch}\beta_n\eta + \cos\beta_n\eta) - \sigma_n(\mathrm{sh}\beta_n\eta + \sin\beta_n\eta) \tag{26}$$

where

$$\sigma_n = \frac{\mathrm{ch}\beta_n - \cos\beta_n}{\mathrm{sh}\beta_n - \sin\beta_n}, \qquad n = 3,4,5,\ldots \tag{27}$$

$m,n = 1$ and 2 correspond to the rigid body translation and the rigid body rotation of a free-free beam, respectively, and $m,n = 3$ corresponds to the lowest bending mode of the beam. For the plate, an odd number n corresponds to a symmetric mode with respect to the center axis of the plate in the direction of load, $y = b/2$, and an even number n corresponds to an antisymmetric mode with respect to that axis. It is clear that the functions (20–27) satisfy the following conditions:

$$\int_0^1 \overline{X_m(\xi)}\, d\xi = 0, \qquad m = 2,3,4,\ldots \tag{28}$$

$$\int_0^1 \overline{Y_n(\eta)}\, d\eta = 0, \qquad n = 2,3,4,\ldots \tag{29}$$

$$\int_0^1 \overline{X_m(\xi)}\,\overline{X_i(\xi)}\, d\xi = \delta_{mi}, \qquad m,i = 1,2,3,\ldots \tag{30}$$

$$\int_0^1 \overline{Y_n(\eta)}\,\overline{Y_j(\eta)}\, d\eta = \delta_{nj}, \qquad n,j = 1,2,3,\ldots \tag{31}$$

where δ_{mi} and δ_{nj} are Kronecker's deltas. By using Eqs. (17–31) in Eqs. (9–11), we can define the following coefficients:

$$\overline{M_{mnij}} = \delta_{mi}\,\delta_{nj} \tag{32}$$

$$\begin{aligned}\overline{K_{mnij}} = {} & \int_0^1 \overline{X_m''}\,\overline{X_i''}\, d\xi\, \delta_{nj} \\ & + \lambda^2[2(1-\nu)\int_0^1 \overline{X_m'}\,\overline{X_i'}\, d\xi \int_0^1 \overline{Y_n'}\,\overline{Y_j'}\, d\eta \\ & + \nu(\int_0^1 \overline{X_m''}\,\overline{X_i}\, d\xi \int_0^1 \overline{Y_n}\,\overline{Y_j''}\, d\eta \\ & + \int_0^1 \overline{X_m}\,\overline{X_i''}\, d\xi \int_0^1 \overline{Y_n''}\,\overline{Y_j}\, d\eta)] \\ & + \lambda^4\,\delta_{mi}\int_0^1 \overline{Y_n''}\,\overline{Y_j''}\, d\eta\end{aligned} \tag{33}$$

$$\overline{G_{mnij}} = [(\Theta + 1)\overline{X_m'}\,\overline{X_i}\,|_{\xi=1} - \xi\overline{X_m'}\,\overline{X_i'}\, d\xi]\,\delta_{nj} \tag{34}$$

Eigenvalue Equations

Now the eigenvalue problem, Eq. (16), can be written, by using Eqs. (32–34), as follows:

$$\sum_m \sum_n \overline{W_{mn}}(-\Omega^2\,\overline{M_{mnij}} + \overline{K_{mnij}} + Q\,\overline{G_{mnij}}) = 0$$

$$m,n,i,j = 1,2,3,\ldots \tag{35}$$

where

$$\Omega^2 = \bar{m}\omega^2 a^4/D \tag{36}$$

and

$$Q = qa^2/D \tag{37}$$

are introduced as the nondimensional frequency square and the nondimensional load, respectively.

In this study, we use the coordinate functions up to the eighth mode in each direction. For nontrivial solutions of this eigenvalue problem, Eq. (35), we finally obtain the following eigenvalue equations:

$$\det(-\Omega^2\,\overline{M_{mnij}} + \overline{K_{mnij}} + Q\,\overline{G_{mnij}}) = 0$$

$$m,n,i,j = 1,2,3,\ldots, 8 \tag{38}$$

In the present paper, the direction parameter of the follower force Θ is set to zero, which corresponds to a purely tangential follower force case.

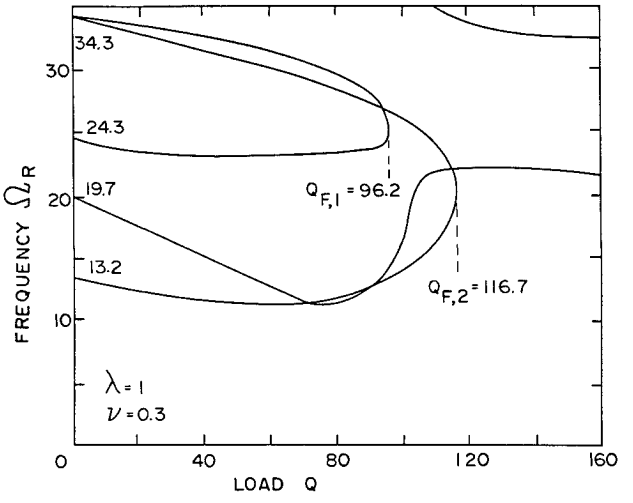

Fig. 2 Eigenvalue curves ($\lambda = 1$, $\nu = 0.3$).

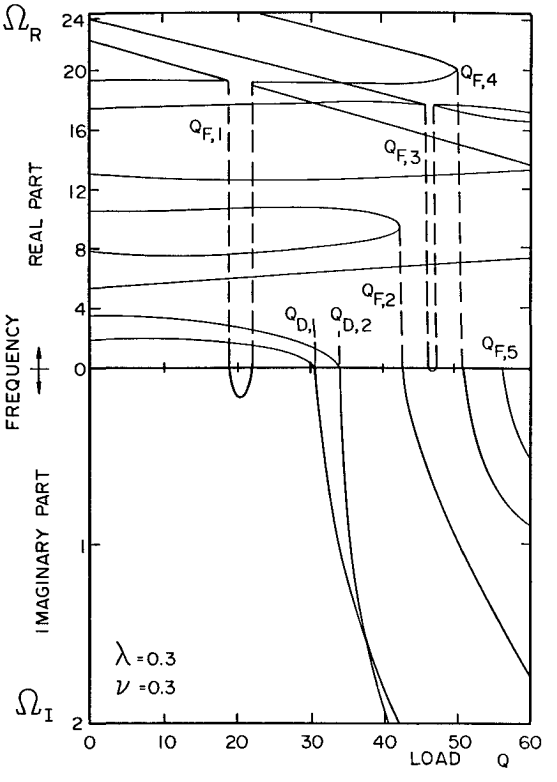

Fig. 3 Eigenvalue curves ($\lambda = 0.3$, $\nu = 0.3$).

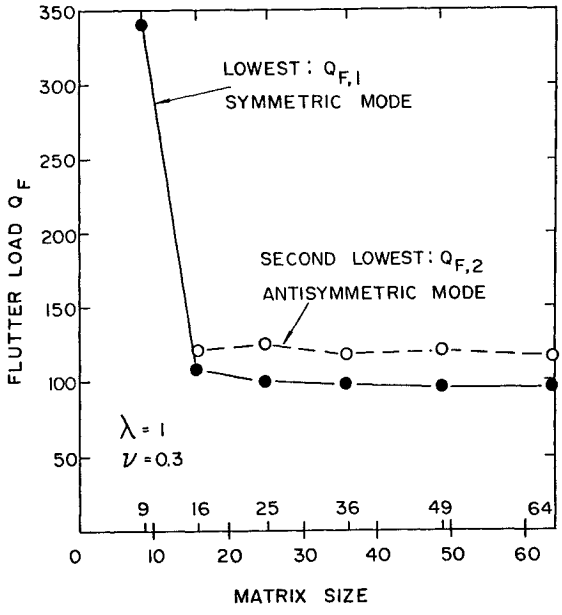

Fig. 4 Convergence of flutter load with number of modes used in the analysis.

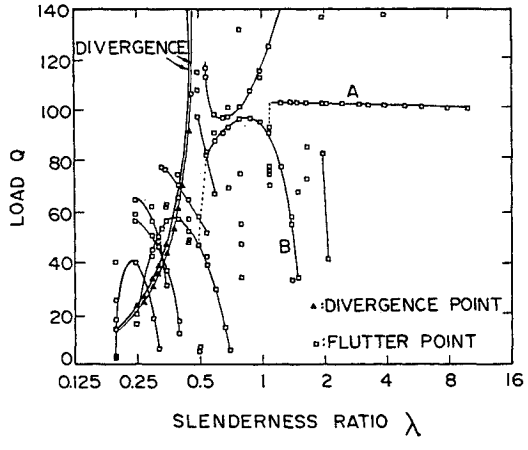

Fig. 5 Flutter load and divergence load vs slenderness ratio.

III. Results

Eigenvalue Curves

Examples of the eigenvalue curves are shown in Figs. 2 and 3. Figure 2 is for the case of square plate, i.e., $\lambda = 1$. Flutter occurs when two real frequencies merge into a pair of complex frequencies. Divergence occurs when a real frequency becomes zero. These phenomena are clearly shown in Fig. 3 for the case of $\lambda = 0.3$. In this figure, $Q_{D,1}$ and $Q_{D,2}$ denote divergence loads, $Q_{F,2}$ and $Q_{F,4}$ show strong flutter loads, and $Q_{F,1}$ and $Q_{F,3}$ show weak flutter instabilities. The figure shows that $Q_{F,5}$ corresponds to flutter of a much higher (frequency) mode. The weak instability $Q_{F,1}$, not the strong flutter load $Q_{F,2}$ for a lower mode nor the divergence load $Q_{D,1}$, is the critical load in this case.

There are altogether 64 frequencies in the model used for the calculations. The lowest three frequencies of the free rectangular plate for $\Theta = 0$ are always equal to zero, corresponding to rigid body modes. It is assumed that the rigid body modes can be controlled properly and do not cause any destructive behavior of the structure. So, the rigid body modes are not illustrated in the eigenvalue curves.

Figure 4 shows the convergence of flutter load for a square plate with respect to the number of modes applied. Taking up to the eighth mode in each direction, which means a 64×64 matrix size, appears to be enough to ensure convergence.

Weak Instabilities

Divergence load and flutter load for various slenderness ratios of the rectangular plate are shown in Fig. 5. Divergence loads for symmetric and antisymmetric modes show smooth behavior as the slenderness ratio changes. On the other hand, flutter loads sometimes change abruptly as the slenderness ratio changes. The flutter mechanism is very sensitive to a change of slenderness ratio. This is because there exist many weak instabilities due to higher modes and there may be a change in the most critical flutter mode due to a change in slenderness ratio. And these weak instabilities sometimes determine the critical load for a given slenderness ratio as shown in Fig. 5, and more clearly as previously shown in Fig. 3.

However, it is possible to identify smooth envelopes of flutter loads for similar eigenmodes. Flutter points that are not connected by envelope curves in Fig. 5 correspond to extremely weak instabilities or weak instabilities of much higher modes. An envelope curve, written as A in Fig. 5, changes abruptly at its left end into an envelope curve, written

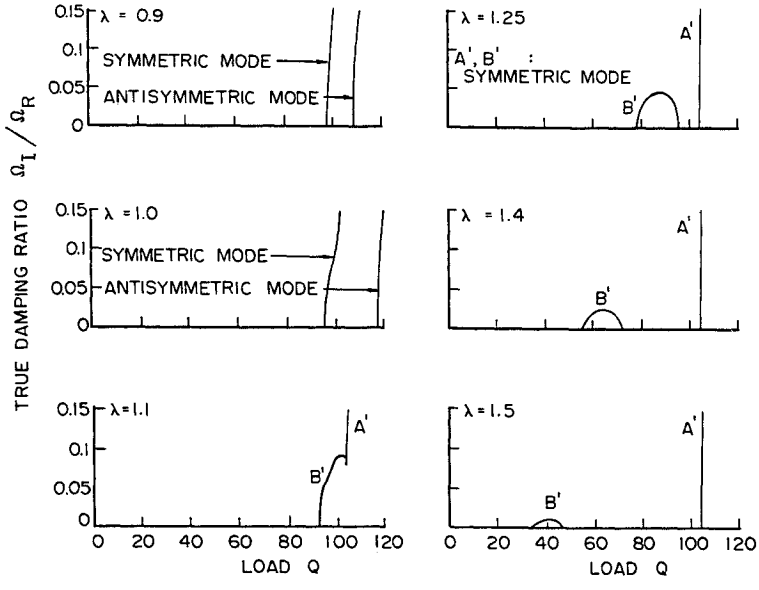

Fig. 6 Intensity of flutter and its transition.

as B, with a drastic change of flutter load. On the other hand, the right end of the envelope curve B decreases sharply as the slenderness ratio increases. The reason for this behavior is explained as follows and is illustrated in Figs. 6 and 7.

The ordinate Ω_I/Ω_R in Fig. 6 is a measure of the intensity of flutter, which involves the true damping ratio,[21] where Ω_I and Ω_R are the imaginary and real parts of the nondimensional frequency, respectively. There is a strong instability noted as A′ and a weak instability noted as B′ in each figure for the cases of a slenderness ratio larger than about 1.1. In Fig. 6, A′ and B′ correspond to A and B in Fig. 5, respectively. There occurs a linked shape of A′ and B′ for the case of slenderness ratio 1.1. The linked shape separates into A′ and B′ for a slenderness ratio larger than about 1.25. This link is the reason for the abrupt change of flutter load at the merging point of envelope curves A and B in Fig. 5.

The weak instability B′ becomes weaker, and at the same time it occurs at lower load, as the slenderness ratio increases, as shown in Fig. 6. The reason for this tendency can be understood as follows. Figure 7 shows the natural frequencies without loading for the lowest several modes. The numbers *m* and *n* in the parentheses in Fig. 7 denote the dominant primitive modes shown in Eqs. (20-22) and Eqs. (24-26), respectively. The most critical two modes in this figure are modes C and D. Both modes C and D are for symmetric deflection, as noted from *n* in the parentheses in the figure. Moreover, both change their natural frequencies monotonically, as the slenderness ratio changes. But, as shown by the mode number *m* in the parentheses, mode D is a higher bending mode in the direction of loading than mode C.

Now recall that for a certain load, mode D merges into mode C, which means flutter or a weak instability, Figs. 2 and 3. Secondly, note that the increase of nondimensional frequency for mode D due to an increase of slenderness ratio has a limit, Fig. 7. However, the nondimensional frequency for mode C is almost linear with respect to an increase of slenderness ratio. Therefore, the difference between the two frequencies for modes C and D becomes smaller as the slenderness ratio increases. Thus, with increasing slenderness ratio, the two modes can merge more easily into an instability. However, the intensity of the instability becomes weaker; this weak instability disappears at the intersection of the two modes C and D.

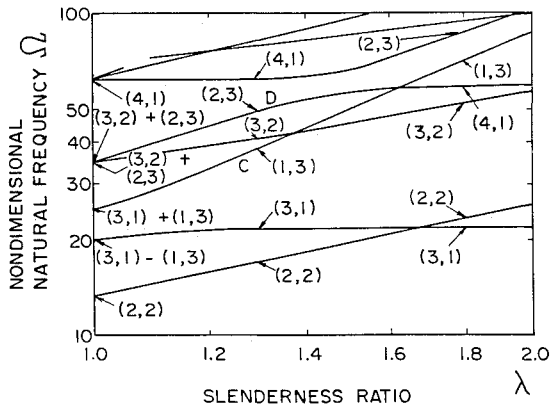

Fig. 7 Change of natural frequency with slenderness ratio for no force (lower 4th to 11th frequencies).

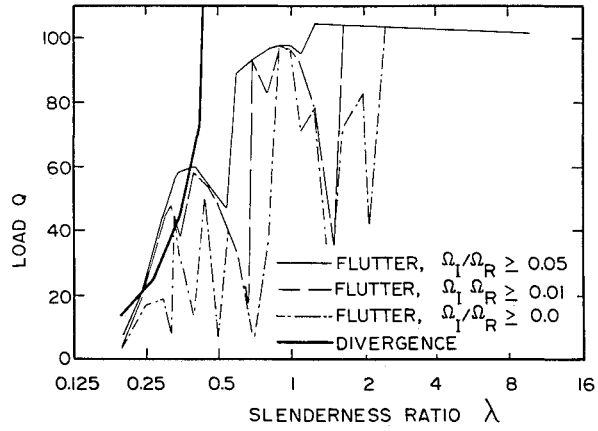

Fig. 8 Flutter load and divergence load for various true damping ratios.

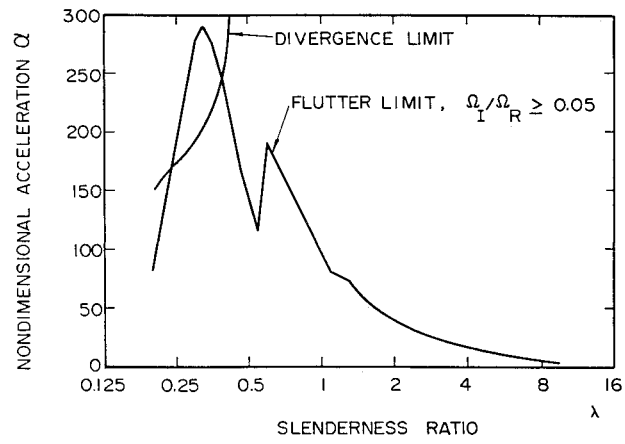

Fig. 9 Flutter acceleration and divergence acceleration vs slenderness ratio.

Damping

As shown in Fig. 5, the lowest instability load may change abruptly due to a change of slenderness ratio if there is no damping. In the presence of structural damping, some of the weak instabilities disappear. A perturbation analysis shows that the true damping ratio Ω_I/Ω_R, is approximately equivalent to one-half of a structural damping coefficient g.[21] It is expected, therefore, from Fig. 6 that a weak instability whose intensity is smaller than a certain level of true damping ratio will not occur for sufficiently large g. The lowest flutter load and divergence load are shown in Fig. 8 for three values of Ω_I/Ω_R or $g/2$: 0, 0.01, and 0.05. In the case of $\Omega_I/\Omega_R \geq 0.05$, the flutter load variation with slenderness ratio is comparatively smooth. Moreover, there is no significant change in the nature of this variation if the threshold of Ω_I/Ω_R is increased beyond 0.05.

Acceleration Limits

In the application of these results to the optimum design of a large space structure, the best choice of slenderness ratio for a rectangular plate will be desired. This choice may be defined, for example, as the maximum in-plane rigid body acceleration of the plate for which no instability occurs for a given total area of a rectangular plate. Toward this end, based upon the condition that the area is held constant, the nondimensional acceleration α is defined here as

$$\alpha = \frac{qb/\bar{m}ab}{D/\bar{m}(ab)^{3/2}} = \frac{Q}{\lambda^{3/2}} \tag{39}$$

where $qb/(\bar{m}ab)$ is the actual acceleration of the plate, Q is the nondimensional load, and λ is the slenderness ratio. The lowest flutter acceleration and the lowest divergence acceleration for various slenderness ratios are shown in Fig. 9. The threshold of Ω_I/Ω_R for flutter in this figure is 0.05. It is seen that a smaller slenderness ratio is generally desirable and that there exist maximal values around $\lambda = 0.4$ and 0.6. However, the rapid change of the results of flutter limit and divergence limit in that slenderness ratio range, 0.4 to 0.6, may require special attention in actual applications.

IV. Concluding Remarks

Flutter and divergence loads of flexible rectangular plates with free edges subjected to a follower force were obtained for various slenderness ratios. The flutter mechanism was studied closely because the behavior of flutter is fairly complicated. Many weak instabilities were found. The weak instability sometimes determines the critical load, which is often significantly smaller than the strong flutter load or the divergence load. Therefore, critical loads show a rapid variation with a change of slenderness ratio for zero structural damping. However, some instabilities do not occur if damping exists.

A slenderness ratio near 0.4 or 0.6 is desirable from the viewpoint of obtaining a large in-plane rigid body acceleration caused by the thrust without flutter or divergence. However, the rapid variation of the minimum acceleration at which flutter occurs in this slenderness ratio range may suggest that caution is needed in using these results.

Acknowledgment

This work was supported, in part, by Army Research Office Contract DAAL03-87-K-0023. Gary Anderson is the Technical Monitor.

References

[1]Beal, T. R., "Dynamic Stability of a Flexible Missile under Constant and Pulsating Thrust," *AIAA Journal,* Vol. 3, No. 3, 1965, pp. 486-494.

[2]Walter, W. W., and Anderson, G. L., "Stability of a System of Three Degrees of Freedom Subjected to a Circulatory Force," *Journal of Sound and Vibration,* Vol. 45, No. 1, 1976, pp. 105-114.

[3]Wu, J. J., "On Missile Stability," *Journal of Sound and Vibration,* Vol. 49, No. 1, 1976, pp. 141-147.

[4]Peters, D. A., and Wu, J. J., "Asymptotic Solutions to a Stability Problem," *Journal of Sound and Vibration,* Vol. 59, No. 4, 1978, pp. 591-610.

[5]Matsumoto, G. Y., and Mote, C. D., Jr., "Time Delay Instabilities in Large Order Systems With Controlled Follower Forces," *Transactions of the ASME, Journal of Dynamic Systems, Measurements, and Control,* Vol. 94, No. 4, 1972, pp. 330-334.

[6]Park, Y. P., and Mote, C. D., Jr., "The Maximum Controlled Follower Force on a Free-Free Beam Carrying a Concentrated Mass," *Journal of Sound and Vibration,* Vol. 98, No. 2, 1985, pp. 247-256.

[7]Park, Y. P., "Dynamic Stability of a Free Timoshenko Beam Under a Controlled Follower Force," *Journal of Sound and Vibration,* Vol. 113, No. 3, 1987, pp. 407-415.

[8]Celep, Z., "On the Stability of a Discrete Model of the Free-Free Beam Subjected to End-Loads," *Journal of Sound and Vibration,* Vol. 59, No. 1, 1978, pp. 153-157.

[9]Celep, Z., "On the Vibration and Stability of a Free-Free Beam Subjected to End-Loads," *Journal of Sound and Vibration,* Vol. 61, No. 3, 1978, pp. 375-381.

[10]Celep, Z., "Axially Symmetric Stability of a Completely Free Circular Plate Subjected to a Non-Conservative Edge Load," *Journal of Sound and Vibration,* Vol. 65, No. 4, 1979, pp. 549-556.

[11]Celep, Z., "Vibration and Stability of a Free Circular Plate Subjected to a Non-Conservative Loading," *Journal of Sound and Vibration,* Vol. 80, No. 3, 1982, pp. 421-432.

[12]Farshad, M., "Stability of Cantilever plates Subjected to Biaxial Subtangential Loading," *Journal of Sound and Vibration,* Vol. 58, No. 4, 1978, pp. 555-561.

[13]Culkowski, P. M., and Reismann, H., "Plate Buckling Due to Follower Edge Forces," *Transactions of the ASME, Ser. E, Journal of Applied Mechanics,* Vol. 44, 1977, pp. 768-769.

[14]Adali, S., "Stability of a Rectangular Plate Under Nonconservative and Conservative Forces," *International Journal of Solids and Structures,* Vol. 18, No. 12, 1982, pp. 1043-1052.

[15]Leipholz, H. H. E., "Stability of a Rectangular Simply Supported Plate Subjected to Nonincreasing Tangential Follower Forces," *Transactions of the ASME, Ser. E, Journal of Applied Mechanics,* Vol. 45, No. 3, 1978, pp. 223-224.

[16]Leipholz, H. H. E., and Pfendt, F., "On the Stability of Rectangular, Completely Supported Plates with Uncoupling Boundary Conditions Subjected to Uniformly Distributed Follower Forces," *Computer Methods in Applied Mechanics and Engineering,* Vol. 30, 1982, pp. 19-52.

[17]Leipholz, H. H. E., and Pfendt, F., "Application of Extended Equations of Galerkin to Stability problems of Rectangular plates with Free Edges and Subjected to Uniformly Distributed Follower Forces," *Computer Methods in Applied Mechanics and Engineering,* Vol. 37, 1983, pp. 341-365.

[18]Dowell, E. H., "Aeroelasticity of plates and Shells," Noordhoff International publishing, Leyden, 1975, pp. 26-29.

[19]Felgar, R. P., Jr., "Formulas for Integrals Containing Characteristic Functions of a Vibrating Beam," The University of Texas publication, Circular No. 14, 1950.

[20]Young, D., and Felgar, R. P., Jr., "Tables of Characteristic Functions Representing Normal Modes of Vibration of a Beam," The University of Texas publication, Engineering Research Series No. 44, 1949.

[21]Dowell, E. H., Curtiss, H. C., Jr., Scanlan, R. H., and Sisto, F., "A Modern Course in Aeroelasticity," Sijthoff & Noordhoff, Alphen aan den Rijn, 1978, pp. 104-110.